INVARIANCE AND INVERSE STABILITY UNDER RELU

Anonymous authors
Paper under double-blind review

ABSTRACT

We flip the usual approach to study invariance and robustness of neural networks by considering the non-uniqueness and instability of the inverse mapping. We provide theoretical and numerical results on the inverse of ReLU-layers. First, we derive a necessary and sufficient condition on the existence of invariance that provides a geometric interpretation. Next, we move to robustness via analyzing local effects on the inverse. To conclude, we show how this reverse point of view not only provides insights into key effects, but also enables to view adversarial examples from different perspectives.

1 INTRODUCTION

Invariance and stability/robustness are two of the most important properties characterizing the behavior of a neural network. Due to growing requirements like robustness to adversarial examples (Szegedy et al., 2014) and the increasing use of deep learning in safety-critical applications, there has been a surge in interest in these properties. Invariance and stability are considered to be the key mechanisms in dealing with uninformative properties of the input, see e.g. (Achille & Soatto, 2017; Mallat, 2016); also from the information theoretical perspective (Tishby & Zaslavsky, 2015; Saxe et al., 2018) in form of the loss of information about the input.
Invariance and stability are also tightly linked to robustness against adversarial attacks (Cisse et al., 2017; Tsuzuku et al., 2018; Simon-Gabriel et al., 2018), generalization (Sokolić et al., 2017; Gouk et al., 2018) and even the training of Generative Adversarial Networks (Miyato et al., 2018).
In general, stability is studied via two basic properties: 1) locally via the Jacobian (Sokolić et al., 2017; Simon-Gabriel et al., 2018), 2) globally via the Lipschitz constant (Cisse et al., 2017; Miyato et al., 2018; Tsuzuku et al., 2018). From a high-level perspective both of these approaches study an upper bound on stability as the Lipschitz constant as well as the gradient correspond to the highest possible responds for a given perturbation. We, unlike the approaches above, aim to broaden our understanding by analyzing the lowest possible response.
More formally, we study which perturbations Δx do not (or only little) affect the outcome of a network F. Our analysis considers a given input data point x and investigates the Δx's, such that

$$F(x) = F(x + \Delta x) \quad \text{(invariant)} \qquad \text{or} \qquad \|F(x) - F(x + \Delta x)\| \leq \varepsilon \quad \text{(stable)},$$

where a small $\varepsilon > 0$ is given. These properties can be crucial for many discriminative tasks in order to contract the space along (for the output) uninformative directions (Mallat, 2016). However, a model would be flawed if perturbations that alter the semantics have only a minor impact on the features and thereby on the output of the network. This is the reverse perspective to the common one on adviserial examples (Szegedy et al., 2014), which considers small input perturbations that lead to large changes and thus to arbitrary decisions of the network.
This flipped view and the study of lowest response calls for a different approach: we study the instabilities of the inverse instead of the stabilities of the forward mapping. In particular, if F is invariant to perturbations Δx, then x and $x + \Delta x$ lie in the preimage of the output $z = F(x)$ i.e. F is not uniquely invertible. Robustness towards large perturbations induces an instable inverse mapping as small changes in the output can be due to large changes in the input. In summary, our analysis flips the perspective on invariance and stability and applies this new point of view to ReLU-layers.
Our contributions are as follows:

- We derive conditions when the preimage of an output of a ReLU-layer is finite, infinite, or a single point. Based on these conditions, we derive an algorithm to check these conditions and exemplify its usability by applying it to investigate the preimages of a trained network. (See Section 2.)

- We study the stability of the inverse via analyzing the linearization at a point in input space, which is accurate within a polytope. We provide upper bounds on the smallest singular value and prove how the removal of uncorrelated features could effect the stability of the inverse mapping. Based on these ideas, we experimentally demonstrate how singular values evolve over the different layers in rectifier networks. (See Section 3.)
- We connect our reverse view on adversarial examples to invariance and robustness by leveraging our analysis of preimages. (see Section 5)

1.1 Related Work

While analyzing invariance and robustness properties is a major topic in theoretical treatments of deep networks (Mallat, 2016), studying it via the inverse is less common. Several works like Mahendran & Vedaldi (2015), Mahendran & Vedaldi (2016) or Dosovitskiy & Brox (2016) focus on reconstructing inputs from features of convolutional neural networks (CNNs) to visualize the information content of features. Instead, we investigate potential mechanisms affecting the invertibility.
Carlsson et al. (2017) gives a first geometrical view on the shape of preimages of outputs from ReLU layers, which is directly related to the question of injectivity of the mapping under ReLU. Shang et al. (2016) analyzes the reconstruction property of cReLU (concatenated ReLU); however, the more general situation of using the standard rectifier is not studied. A notable other line of work assumes random weights in order to derive guarantees for invertibility, see Gilbert et al. (2017) or Arora et al. (2015), whereas we aim to theoretically derive means to uncover mechanisms of rectifier networks without assumptions on the weights.
Moreover, several reversible network structures were recently proposed (Gomez et al., 2017; Chang et al., 2018; Jacobsen et al., 2018). Most notably, in Jacobsen et al. (2018) a bijective network, up to its last layer, was trained successfully on ImageNet which does not exhibit any invariance. However, the network is very robust towards many directions in the input which is reflected in a strongly instable inverse. Hence, even carefully designed network show at least one of the two effects (invariance and robustness) studied in this work. Especially stability has seen growing interest due to adversarial examples (Szegedy et al., 2014), yet stability is mostly studied with respect to the forward mapping, see e.g. Cisse et al. (2017).
Two main resources for our view of rectifier networks as piecewise linear models are Montufar et al. (2014) and Raghu et al. (2017). Closest to our approach is the work of Bruna et al. (2014) on global statements of injectivity and stability of a single layer including ReLU and pooling. The authors focus on global injectivity and stability bounds via combinatorial statements over all configurations attainable by ReLU and pooling. These conditions are valid on the entire input space, while the restriction to parts of the input space may be far from these worst-case conditions.
Further works focus on applications like inverse problems with learned forward models (Jensen et al., 1999; Lu et al., 1999) and parameter estimation problems (Lähivaara et al., 2018), which are often formulated as inverse problems and require the inversion of networks.

1.2 Notation

- Input: $x = x^0 \in \mathbb{R}^{d_0}$, sometimes shortened to $d := d_0$.
- Pre-activations: $z^l = A^l x^{l-1} + b^l \in \mathbb{R}^{d_l}$, with weight matrix $A^l \in \mathbb{R}^{d_l \times d_{l-1}}$ and bias $b^l \in \mathbb{R}^{d_l}$.
- Activation: $x^l = \phi(z^l) \in \mathbb{R}^{d_l}$, where $\phi : \mathbb{R} \to \mathbb{R}$ the pointwise applied activation function, if not specified differently $g := \mathrm{ReLU}$.
- Number of layers: $L \in \mathbb{N}$
- Entire network: $F : \mathbb{R}^d \ni x \mapsto F(x) := z := z^L \in \mathbb{R}^{d_L}$, sometimes short $D := d_L$.

For matrices $A \in \mathbb{R}^{m \times n}$ and $I \subset [m] := \{1, \dots, m\}$, $A|_I$ denotes the matrix consisting of the rows of A whose index is in set I – analogously for vectors. Also $A|_{y>0}$ describes the restriction to the index set $\{i : y_i > 0\}$ for $y \in \mathbb{R}^m$, analogously for $<, =, \leq, \geq$. For vectors $y \in \mathbb{R}^m$, $y > 0$ is the elementwise relation, analogously for $<, =, \leq, \geq$. Furthermore, we define $\mathcal{N}(A)$ as the null space of a matrix A. The Euclidean inner product is denoted by $\langle \cdot, \cdot \rangle$.
For every matrix $A \in \mathbb{R}^{m \times n}$ with the rows a_i, $i \in [m]$, we associate the set $A = \{a_i\}_{i=1}^m$. Vice versa, we associate every finite set in $\mathbb{R}^n$ with a matrix (only possible up to permutation of the indices).

Figure 1: Gray lines are hyperplanes with normal vectors (arrows) from the rows of A and translation b. Left: Omnidirectional tuple (A, b) for $p \in \mathbb{R}^2$, as hyperplanes intersect in p and normal vectors are omnidirectional. Two in the middle: Intersection in p, but vector-free halfspaces (hence, not omnidirectional). Right: hyperplanes do not intersect in a point, but normal vectors are omnidirectional.

2 Preimages of ReLU Layer

2.1 Theoretical Analysis

In this section, we analyze different kinds of preimages of a ReLU-layer and investigate under which conditions the inverse image of a given point is a singleton (a set containing exactly one element) or has finite/infinite volume. These conditions will yield a simple algorithm able to distinguish between these different preimages, which is applied in Section 2.2.
For the analysis of pre-images of a given output one can study single layers separately or multiple layers at once. However, since the concatenation of two injective functions is again injective while a non-injective function followed by an injective function is non-injective, studying single layers is crucial. We therefore develop a theory for the case of single layers in this section. Notice that in case of multiple layers one is also required to investigate the image space of the previous layer.
We will focus our study on the most common activation function, ReLU. One of its key features is the non-injectivity, caused by the constant mapping on the negative half space. It provides neural networks with an efficient way to deploy invariances. Basically all other common activation functions are injective, which would lead to a straightforward analysis of the preimages. However, injective activations like ELU (Clevert et al., 2016) and Leaky ReLU (Maas et al., 2013) only swap the invariance for robustness, which in turn leads to the problem of having instable inverses. This question of stability will be analyzed in more detail in Section 3.
We start by introducing one of our main tools – namely the *omnidirectionality*.

Definition 1 (Omnidirectionality)

i) *$A \in \mathbb{R}^{m\times n}$ is called omnidirectional if there exists a unique $x \in \mathbb{R}^n$, such that $Ax \leq 0$.*

ii) *$A \in \mathbb{R}^{m\times n}$ and $b \in \mathbb{R}^m$ are called omnidirectional for the point $p \in \mathbb{R}^n$ if A is omnidirectional and $b = -Ap$.*

Corollary 2 *The following statements are equivalent:*

i) *$A \in \mathbb{R}^{m\times n}$ is omnidirectional.*

ii) *There exist no $x \in \mathbb{R}^n \setminus \{0\}$, such that $Ax \leq 0$.*

iii) *Every linear open halfspace in $\mathbb{R}^n$ contains a row of A.*

iv) *$Ax \leq 0$ implies $x = 0$, where $x \in \mathbb{R}^n$.*

The short proofs of the statements in Corollary 2 are provided in Appendix A1.
Thus, for every direction of a hyperplane through the origin forming two halfspaces, there is a vector from the rows of A inside each open halfspace, hence the term *omnidirectional* (see Figure 1 for an illustration). Note that the hyperplanes are due to ReLU as it maps the open halfspace to positive values and the closed halfspace to zero. A straightforward way to construct an omnidirectional matrix is by taking a matrix whose rows form a spanning set $\mathcal{F}$ and use the vertical concatenation of $\mathcal{F}$ and $-\mathcal{F}$. This idea is realated to cReLU (Shang et al., 2016).
More importantly, omnidirectionality is directly related to the ReLU-layer preimages and will provide us with a computable method to characterize their volume (see Theorem 4). To analyze such inverse images, we consider $y = \mathrm{ReLU}(Ax + b)$ for a given output $y \in \mathbb{R}^m$ with $A \in \mathbb{R}^{m\times n}$, $b \in \mathbb{R}^m$ and

$x \in \mathbb{R}^n$. If we know A, b and y, we can write the equation as the following mixed linear system:

$$A|_{y>0}x + b|_{y>0} = y|_{y>0} \tag{1}$$
$$A|_{y=0}x + b|_{y=0} \leq 0. \tag{2}$$

Remark 3 *It is possible to enrich the mixed system to include conditions/priors on x (e.g. $x \in \mathbb{R}^n_{\geq 0}$).*

The inequality system in equation 2 links its set of solutions and therefore the volume of the preimages of the ReLU-layer with the omnidirectionality of A and b. Defining $\overline{A} := AO^T$, where $O \in \mathbb{R}^{k \times n}$ denotes an orthonormal basis of $\mathcal{N}(A|_{y>0})$ with $k := \dim \mathcal{N}(A|_{y>0})$ and $\overline{b} := b|_{y\leq 0} + A|_{y\leq 0}(P_{\mathcal{N}(A|_{y>0})^\perp}x)$, where P_V denotes the orthogonal projection into the closed space V, leads to the following main theorem of this section, which is proven in Appendix A1.

Theorem 4 (Preimages of ReLU- layer) *The preimage of a point y under a ReLU-layer is*

i) *for $k = 0$ a singleton.*

ii) *for $k > 0$ a singleton, if and only if there exists an index set I for the rows of $\overline{A}$ and $\overline{b}$, such that $(\overline{A}|_I, \overline{b}|_I)$ is omnidirectional for some point $p \in \mathbb{R}^k$.*

iii) *for $k > 0$ a compact polytope with finite volume, if and only if $\overline{A}$ is omnidirectional.*

Thus, omnidirectionality allows in theory to distinguish whether the inverse image of a ReLU-layer is a singleton, a compact polytope or has infinite volume. However, obtaining a computable method to decide whether a given matrix is omnidirectional is crucial for later numerical investigations. For this reason, we will go back to the geometrical perspective of omnidirectionality (see Figure 1). This will also help us to get a better intuition on the frequency of occurence of the different preimages. The following Theorem 5 gives another geometrical interpretation of omnidirectionality besides Corollary 2iii, whose short proof is given in Appendix A1.

Theorem 5 (Convex hull) *A matrix $A \in \mathbb{R}^{m \times n}$ is omnidirectional if and only if $0 \in \mathrm{Conv}(A)^{\mathrm{o}}$, where $\mathrm{Conv}(A)^{\mathrm{o}}$ is the interior of the convex hull spanned by the rows of A (see Definition 10 in Appendix A1).*

Therefore, the matrix must contain a simplex in order to be omnidirectional, as the convex hull of the matrix $A \in \mathbb{R}^{m \times n}$ has to have an interior. Hence, we have the following:

Corollary 6 *If $A \in \mathbb{R}^{m \times n}$ is omnidirectional, then $m > n$.*

By considering the geometric perspective, a tuple $(A \in \mathbb{R}^{m \times n}, b \in \mathbb{R}^m)$ is omnidirectional for a point $p \in \mathbb{R}^n$, if and only if the m hyperplanes generated by the rows of A with bias b intersect at p and their normal vectors (rows of A) form an omnidirectional set. We can use Corollary 6 to conclude that singleton preimages of ReLU-layers are very unlikely to happen in practice (if we do not design for it), since a necessary condition is that $n + 1$ hyperplanes have to intersect in one point in $\mathbb{R}^n$. Therefore we conclude, that singleton preimages of ReLU layers in practice only and exclusively occurs, if the mixed linear system already has sufficient linear equalities.
Furthermore, the above results can be used to derive an algorithm to check whether a preimage of a given output is finite, infinite or just a singleton. A singleton inverse image is obtained as long as $\mathrm{rank}(A|_{y>0}) = n$ holds true, which can be easily computed. To distinguish preimages with finite and infinite volumes, it is enough to check if $\overline{A}$ is omnidirectional (see Theorem 4iii), which can be done numerically by using the definition of the convex hull, Theorem 5 and Corollary 6. This leads to a *linear programming problem*, which is presented in Appendix A3.

2.2 Numerical Analysis

In this section, we demonstrate for a simple model that the preimage of a layer can be a singleton, infinite or finite depending on the given point. For this purpose, we trained a MLP with two hidden ReLU layers of size 3500 and 784 on MNIST (LeCun & Cortes, 2010). We chose the layer size of 3500, because the likelihood of having roughly 784 (input dimension of MNIST) positive outputs was high for this setting. In Figure 3, we plotted the number of samples in the test set that have

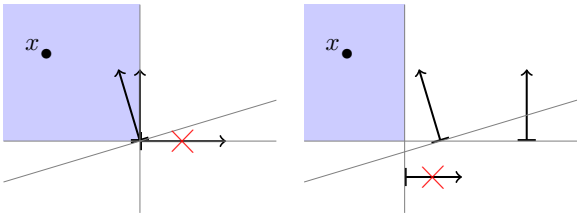

Figure 2: Removal of vectors due to ReLU (red crosses) for the marked points x (left:unbiased setting, right: biased setting). The remaining vectors are only weakly correlated to the removed one, thus yielding an unstable inverse.

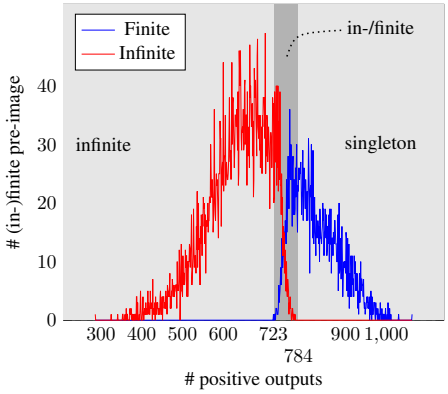

Figure 3: The number of (in-)finite volumed preimages of a ReLU layer over the test set of MNIST. Only within the gray strip we see finite and infinite volumed preimages.

infinite (red curve) or finite (blue curve) preimages over the number of positive outputs. It can be assumed that all samples which have more or equal to 784 (the input dimension) positive outputs have a singleton preimage and are therefore finite. In the dark gray region between 723 and 784, both effects occurred, which can be seen by the overlap of the red and blue curve.
To determine whether a preimage for less than 784 positive outputs was compact we used Theorem 4iii and the algorithm described in Appendix A3.

3 Stability

3.1 Theoretical Analysis

In this section we analyze the robustness of rectifier MLPs against large perturbations via studying the stability of the inverse mapping. Concretely, we study the effect of ReLU on the singular values of the linearization of network F. While the linearization of a network F at some point x only provides a first impression on its global stability properties, the linearization of ReLU networks is exact in some neighborhood due to its piecewise-linear nature (Raghu et al., 2017). In particular, the input space $\mathbb{R}^d$ of a rectifier network F is partitioned into convex polytopes P_F, corresponding to a different linear function on each region. Hence, for each polytope P in the set of all input polytopes P_F, the network F can be simplified as $F(x) = A_P x + b_P$ for all $x \in P$.
Additionally, each of these matrices A_P can be written via a chain of weight matrix multiplications incorporating the effect of ReLU, see Wang et al. (2016). In particular let D_I denote a diagonal matrix with $D_{ii} = 1$ for $i \notin I$ and $D_{ii} = 0$ for $i \in I$. Then A_P of a network with L layers can be written as $A_P = A^L D_{I^{L-1}} A^{L-1} \cdots D_{I^1} A^1$, where A^l are the weight matrices of layer l and $I^l := \{i \in [d_l] : (A^l x^{l-1} + b^l)_i \leq 0\}$. Thus, the effect of ReLU is incorporated in the diagonal matrices D_{I^l} which set the rows of A^l with indices from I^l to zero. For the purpose of studying all possible local behaviors, we define admissible index sets I^l following, with slight modifications, Bruna et al. (2014):

Definition 7 *(Admissible index sets)*
An index set I^l for a layer l is admissible if

$$\bigcap_{i \notin I^l} \{x^l : \langle x^l, a_i^l \rangle > -b_i\} \cap \bigcap_{i \in I^l} \{x^l : \langle x^l, a_i^l \rangle \leq -b_i\} \neq \emptyset.$$

Of special interest for such an analysis is the range of possible effects by the application of the rectifier. Since the effect by ReLU corresponds to the application of D_I for admissible I, we now turn to studying the changes of the singular values due to D_I. By considering the matrix A, e.g.

representing the chain of matrix products up to layer l, the effect of ReLU can be globally upper bounded:

Lemma 8 *(Global upper bound for largest and smallest singular value)*
Let σ_l be the singular values of $D_I A$. Then for all admissible index sets I, the smallest non-zero singular value is upper bounded by $\min\{\sigma_l : \sigma_l > 0\} \leq \tilde{\sigma}_k$, where $k = N - |I|$ and $\tilde{\sigma}_1 \geq ... \geq \tilde{\sigma}_N > 0$ are the non-zero singular values of A.
Furthermore, the largest singular value is upper bounded by $\max\{\sigma_l : \sigma_l > 0\} \leq \tilde{\sigma}_1$.

Lemma 8 analyzes the best case scenario with respect to the highest value of the smallest singular value. While this would yield a more stable inverse mapping, one needs to keep in mind that $\mathcal{N}(A_P)$ grows by the corresponding elimination of rows via D_I. Moreover, reaching this bound is very unlikely as it requires the singular vectors to perfectly align with the directions that collapse due to D_i. Thus, we now turn to study effects which could happen locally for some input polytopes P.
An example of a drastic effect through the application of ReLU is depicted in Figure 2. Since one vector is only weakly correlated to the removed vector and the situation is overdetermined, removing this feature for some inputs x in the blue area leaves over the strongly correlated features. While the two singular values of the 3-vectors-system were close to one, the singular vectors after the removal by ReLU are badly ill-conditioned. As many modern deep networks increase the dimension in the first layers, redundant situations as in Figure 2 are common, which are inherently vulnerable to such phenomena. For example, Rodríguez et al. (2017) proposes a regularizer to avoid such strongly correlated features. The following lemma formalizes the situation exemplified before:

Lemma 9 *(Removal of weakly correlated rows)*
Let $A \in \mathbb{R}^{m \times n}$ with rows a_j and $I \subseteq [m]$. For a fixed $k \in I$ let $a_k \in \mathcal{N}(D_I A)^{\perp}$. Moreover, let

$$\forall j \notin I : |\langle a_j, a_k \rangle| \leq c \frac{\|a_k\|_2}{\sqrt{M}}, \tag{3}$$

with $M = m - |I|$ and constant $c > 0$. Then for the singular values $\sigma_l \neq 0$ of $D_I A$ it holds

$$0 < \sigma_K = \min\{\sigma_l : \sigma_l \neq 0\} \leq c.$$

Note that I has to be admissible when considering the effect of ReLU.
Lemma 9 provides an upper bound on the smallest singular value, given a condition on the correlation of all a_j and a_k. However, the condition 3 depends on the number M of remaining rows a_j. Hence, in a highly redundant setting even after removal by ReLU (large N), c needs to be large such that the correlation fulfills the condition. Yet, in this case the upper bound on the smallest singular value, given by c, is high. We discuss this effect further in the Appendix A5.

Effect of multiple layers: We now turn our focus to the effect of multiple layers and ask whether the use of multiple layers results in a different situation than a 1-hidden layer MLP. In particular: Can the application of another layer have a pre-conditioning effect yielding a stable inverse? What happens when we only compose orthogonal matrices which have stable inverses? Note that a way to enforce an approximate orthogonality constraint was proposed for CNNs in Cisse et al. (2017), however only for the filters of the convolution.
For both situations the answer is similar: the nonlinear nature of ReLU induces locally different effects. Loosely speaking, we apply the layer A^l to different linearizations depending on the input region P. Thus, if we choose a pre-conditioner A^l for a specific matrix A_P^{l-1}, it might not stabilize the matrix product for matrices $A_{P^*}^{l-1}$ corresponding to different input polytopes P^*. For the case of composing only orthogonal matrices, consider a network up to layer $l-1$ where the linearization A_P^{l-1} has orthogonal columns (assume the network gets larger, thus A_P^{l-1} has more rows than columns). Then, the application of ReLU in form of $A^l D_{I^l} A_P^{l-1}$ removes the orthogonality property of the rows of A_P^{l-1}, if setting entries in the rows from I^l to zero results in non-orthogonal columns. This effect is likely, especially when considering dense matrices, hence $D_{I^l} A_P^{l-1}$ is for some I^l not orthogonal. Thus, the matrix product $A^l D_{I^l} A_P^{l-1}$ is not orthogonal, resulting in decaying singular values.
This is why, even when especially designing the network by e.g. orthogonal matrices, stability issues with respect to the inverse arise. To conclude this section, we remark that the presented results are

rather of a *qualitative* nature showcasing effects of ReLU on the singular values. Yet, the analysis does not require any assumptions and is thus valid for any MLP (including CNNs without pooling). To give an idea of *quantitative* effects we study numerical examples in the subsequent subsection.

3.2 Numerical Analysis

In this section, we show how the previously discussed theoretical stability properties can be examined for a given network. In particular, we conduct experiments on CIFAR10 Krizhevsky & Hinton (2009) using two baseline CNNs, see A4 for details on architectures and training setup. Our CNNs use only strides instead of pooling and use no residual connections and normalization layers. Thus, the architectures fit to the theoretical study as the strided discrete convolution can be written as a matrix-vector multiplication.

Singular values over multiple layers: Experimentally most interesting is the development of singular values over multiple layer as several effects are potentially at interplay. Figure 5 shows how all singular values evolve in convolutional layers (layers 1-6, after application of ReLU). While the shape of the curve is similar for layer 1-5, it can be seen that the largest singular value grows, while the small singular values decrease significantly. Note that this growth of the largest singular values is in line with observations for adversarial examples, see Szegedy et al. (2014). While many defense strategies like Cisse et al. (2017) or Jia (2017) focus on the largest singular value, the behavior of the smaller singular values is often overlooked. Additionally, we provide in Appendix A5 a numerical analysis of the condition from Lemma 9 to gain an understanding of possible effects of ReLU on the singular values. Furthermore, we add results for a thinner CNN (ThinCIFAR) and for the MLP from Section 2.2 in Appendix A6.

Relationship between stability and invariance: While invariance is characterized by zero singular values, the condition number only takes non-zero singular values into account, see e.g. layer 6 from Figure 5. This tight relationship is further investigated in Figure 4 which compares the output size, the condition number and the number of non-zero singular values vs. the layers for WideCIFAR and ThinCIFAR. In combination with lower output dimension, ReLU has a different effect for ThinCIFAR. The number of singular values decreases in layer 5, which cuts off the smallest singular values, resulting in a lower condition number. Yet, there are more invariance directions within the corresponding linear region.

Computational costs and scaling analysis: First, we remark that the linearization of a network F for an input point x^0 can be computed via backpropagation. Based on this linearization the computation of the full SVD scales cubically. Especially, early CNN-layers have high dimensional outputs which may cause memory issues when computing the entire SVD. We thus choose a small CNN trained on CIFAR10 as these inputs are only of size $32 \times 32 \times 3$. To scale this analysis up to e.g. ImageNet with VGG-networks, a restriction to a window of the input image is necessary to reduce the complexity of the full SVD especially for early layers. See Jacobsen et al. (2018), where the singular values restricted to input windows were used to estimate the stability of the entire i-RevNet trained on ImageNet.

4 Scope

Characterization of preimages over multiple layers: Theorem 4 yields a characterization (singleton, finite, infinite) of the preimage of a point y under a single ReLU-layer. When considering the preimage of y under multiple layers l to $l - i$, two difficulties arise: 1) If the preimage of y under layer l is not a singleton, one needs to compute the intersection of the image of layer $l - 1$ and the preimage of y under layer $l - 1$. 2) For all points in the intersection, the conditions of Theorem 4 need to be checked, which requires the solution of a linear program, see Algorithm 1 in Appendix A3. Hence, our analysis is currently restricted to a layer-by-layer approach. However, this layer-wise and local study could enable to pin down the specific layers where information, which is expressed in non-singleton preimages.

Preimages for convolutional layers: In general, convolutional layers are affine transforms $Ax + b$, but have a sparse and shared structure compared to dense matrices used in MLPs. Thus, the trivial case $rank(A|_{y>0}) = n$ (Algorithm 1, Appendix A3) needs to be explicitly checked. For MLPs it was assumed in section 2.2 that $rank(A|_{y>0}) = |\{i : y_i > 0\}|$ as dense matrix rows are almost surely linear independent in practice.

Inverse stability for convolutional networks: For inverse stability, we consider the linearization

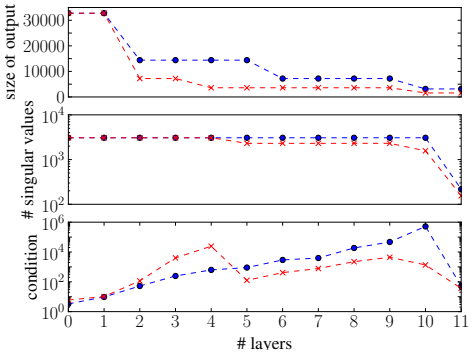

Figure 4: Blue: WideCIFAR, Red: ThinCIFAR. Top: number of output units per layer, Middle: number of singular values, Bottom: Behavior of condition number, each curve over the layers. Here, layers are split into conv-layer and ReLU-activation layer. Singular values and condition number are the median over 50 samples from the CIFAR10 test set.

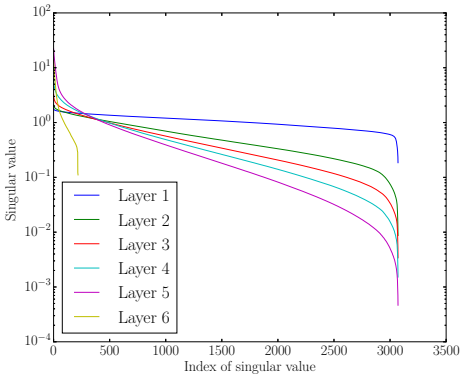

Figure 5: Decay of singular values over the layers of the network. Here, each layer includes the convolution and ReLU-activation. Reported number are taken from median over 50 samples.

$A_P = A^L D_{I^{L-1}} A^{L-1} \cdots D_{I^1} A^1$ for an input polytope P. In convolutional networks, each A^l implements a multi-channel discrete convolution. While singular values of each A^l can be efficiently computed by leveraging the convolutional structure, see (Sedghi et al., 2018), the shared structure is not preserved in the matrix chain A_P due to the application of ReLU (expressed via D_{I^l}). Thus, a tighter analysis that leverages the convolutional structure in A^l, compared to our general assumption that A^l can be any linear mapping, is not straightforward with current tools but would certainly lead to further insights.

Extension of inverse stability across polytopes: In our stability analysis, we employ a piecewise-linear viewpoint which allows to characterize stability via the singular values of the linearization which is exact within an input polytope. However, when considering an ε-ball $B_\varepsilon(y)$ around a point $y = A_P x + b_p$ to model e.g. reconstruction from noisy activations y, further questions arise: 1) Can all points in $B_\varepsilon(y)$ be reached by an x^* from the polytope P? 2) Are points from another polytope P' mapping to points in $B_\varepsilon(y)$? In this case, the inverse stability needs to be augmented by nonlinear considerations to model movements between piecewise-linear regions.

5 Practical Implications

While the focus of this work was an in-depth analysis of potential effects on crucial properties like invariance and robustness due to ReLU, we envision several practical implications of our approach:

Network design and regularization: As both the concept of omnidirectionality and removal of rows due to ReLU showed, there is a breadth of potential effects. In terms of network design, controlling such effects could be desirable. In particular, a change to injective activation functions (tanh, leakyReLU, ELU etc.) remove the discussed pre-images, but immediately transfer to an instable inverse due to saturation. Furthermore, Lemma 9 draws a connection to regularizing correlation between feature maps as introduced in (Rodríguez et al., 2017). Hence, both omnidirectionality and correlation between rows can be thought of as geometrical properties which could partially be controlled by regularization or architecture design.

Furthermore, the analysis also shows the difficulty of controlling these properties in vanilla architectures. However, by incorporating additional structure like dimension splitting in reversible networks (Jacobsen et al., 2018) or invertible residual connections (Behrmann et al., 2018), the preimage is by design a singleton.

Connection to information loss: Our analysis is tightly related to mutual information $I(x^l; x)$ loss, which has gained growing interest due to the information bottleneck (Tishby & Zaslavsky, 2015; Saxe et al., 2018). In particular, invariance in layer l may induce $I(x^l; x) \leq I(x^{l-1}; x)$ due to the data processing inequality (Cover & Thomas, 2006). Similarly, an instable inverse can induce an

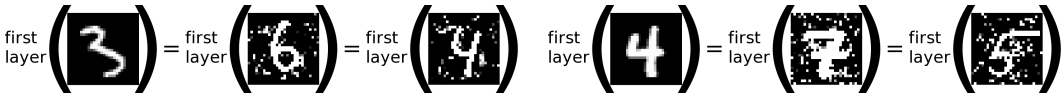

Figure 6: Invariances of the first layer (100 ReLU neurons) of a vanilla multilayer perceptron (MLP). Despite the semantically very different examples, the features are identical as the original image "3" and the two perturbed variants "6" and "4" are in the same preimage. Further details in Appendix A7.

information loss as activations x^l are quantized due to finite precision on hardware.

Implications for adversarial examples: Despite being crucial for many discriminative tasks to contract the space along uninformative directions (Mallat, 2016), invariance and robustness may induce severe vulnerabilities for adversarial examples (Szegedy et al., 2014). For instance, a model would be flawed if perturbations that alter the semantics only have a minor impact on the features of the network. Classically, adversarial examples are viewed as small perturbations which induce large in the network outputs (Goodfellow et al., 2014). Yet, reversing this perspective leads to another failure case: if large changes in the input alter its semantics for a given task, but the networks output is robust or even invariant to such changes, the model might just be as flawed from this reverse point of view.

This change in perspective leads to a natural way of addressing invariance and robustness via invertibility: If F is invariant to perturbations Δx, then x and $x + \Delta x$ lie in the preimage of the output $z = F(x)$ i.e. F is not uniquely invertible. Robustness towards large perturbations induces an instable inverse mapping as small changes in the output can be due to large changes in the input.

Finally Figure 6 demonstrates such a striking failure, where perturbations alter the semantics drastically, yet the activations even after the first layer are identical. To find these examples, we leveraged the developed theory about pre-images and a linear programming formulation, see Appendix A7.

6 Conclusion and Outlook

We presented the inverse as an approach to tackle the invariance and robustness properties of ReLU networks. Particularly, we studied two main effects: 1) conditions under which the preimage of a ReLU layer is a point, finite or infinite and 2) how ReLU can effect the inverse stability of the linearization. By deriving approaches to numerically examine these effects, we highlighted the broad range of possible effects. Moreover, controlling such properties may be desirable as our experiment on adversarial examples showed.

Besides the open questions on how to control such mechanisms via architecture design or regularization, we envision several theoretical directions based on our work. Especially, incorporate nonlinear effects like moving between linear regions of rectifier networks could lift the analysis closer to practice. Furthermore, studying similarities of omnidirectionality as a geometrical property and singular values could further strengthen the link between these two crucial properties.

References

Alessandro Achille and Stefano Soatto. Emergence of invariance and disentangling in deep representations. *arXiv preprint arXiv:1706.01350*, 2017.

Sanjeev Arora, Yingyu Liang, and Tengyu Ma. Why are deep nets reversible: a simple theory, with implications for training. *arXiv preprint*, arXiv:1511.05653, 2015.

Jens Behrmann, David Duvenaud, and Jörn-Henrik Jacobsen. Invertible residual networks. *arXiv preprint arXiv:1811.00995*, 2018.

Joan Bruna, Arthur Szlam, and Yann LeCun. Signal recovery from pooling representations. In *Proceedings of the 31st International Conference on Machine Learning*, 2014.

Stefan Carlsson, Hossein Azizpour, Ali Razavian, Josephine Sullivan, and Kevin Smith. The preimage of rectifier activities. In *International Conference on Learning Representations (workshop)*, 2017.

Bo Chang, Lili Meng, Eldad Haber, Lars Ruthotto, David Begert, and Elliot Holtham. Reversible architectures for arbitrarily deep residual neural networks. *The Thirty-Second AAAI Conference on Artificial Intelligence*, 2018.

François Chollet et al. Keras. `https://github.com/keras-team/keras`, 2015.

Moustapha Cisse, Piotr Bojanowski, Edouard Grave, Yann Dauphin, and Nicolas Usunier. Parseval networks: improving robustness to adversarial examples. In *Proceedings of the 34 International Conference on Machine Learning*, 2017.

Djork-Arné Clevert, Thomas Unterthiner, and Sepp Hochreiter. Fast and accurate deep network learning by exponential linear units (elus). *International Conference on Learning Representations*, 2016.

Thomas M. Cover and Joy A. Thomas. *Elements of Information Theory (Wiley Series in Telecommunications and Signal Processing)*. Wiley-Interscience, New York, NY, USA, 2006.

G.B. Dantzig. *Linear programming and extensions*. Princeton University Press, 1963.

Alexey Dosovitskiy and Thomas Brox. Inverting convolutional networks with convolutional networks. *In Proceedings of IEEE Conference on Computer Vision and Pattern Recognition*, 2016.

Anna Gilbert, Yi Zhang, Kibok Lee, Yuting Zhang, and Honglak Lee. Towards understanding the invertibility of convolutional neural networks. In *26th International Joint Conference on Artificial Intelligence*, 2017.

Aidan N. Gomez, Mengye Ren, Raquel Urtasun, and Roger B. Grosse. The reversible residual network: backpropagation without storing activations. In *Advances in Neural Information Processing Systems 30*, 2017.

Ian Goodfellow, Jonathon Shlens, and Christian Szegedy. Explaining and harnessing adversarial examples. 2014.

Henry Gouk, Eibe Frank, Bernhard Pfahringer, and Michael Cree. Regularisation of neural networks by enforcing lipschitz continuity. *arXiv preprint arXiv:1804.04368*, 2018.

Jörn-Henrik Jacobsen, Arnold W.M. Smeulders, and Edouard Oyallon. i-revnet: deep invertible networks. In *International Conference on Learning Representations*, 2018.

C. A. Jensen, R. D. Reed, R. J. Marks, M. A. El-Sharkawi, Jae-Byung Jung, R. T. Miyamoto, G. M. Anderson, and C. J. Eggen. Inversion of feedforward neural networks: algorithms and applications. In *Proceedings of the IEEE*, volume 87(9), pp. 1536–1549, 1999.

Kui Jia. Improving training of deep neural networks via singular value bounding. *IEEE Conference on Computer Vision and Pattern Recognition*, 2017.

Diederik P. Kingma and Jimmy Ba. Adam: a method for stochastic optimization. *Proceedings of the 32nd International Conference on International Conference on Machine Learning*, 2015.

Alex Krizhevsky and Geoffrey Hinton. Learning multiple layers of features from tiny images, 2009.

Timo Lähivaara, Leo Kärkkäinen, Janne M. J. Huttunen, and Jan S. Hesthaven. Deep convolutional neural networks for estimating porous material parameters with ultrasound tomography. *The Journal of the Acoustical Society of America*, 143(2):1148–1158, 2018.

Yann LeCun and Corinna Cortes. MNIST handwritten digit database, 2010. URL `http://yann.lecun.com/exdb/mnist/`.

Bao-Liang Lu, H. Kita, and Y. Nishikawa. Inverting feedforward neural networks using linear and nonlinear programming. *IEEE Transactions on Neural Networks*, 10(6):1271–1290, 1999.

Andrew L Maas, Awni Y Hannun, and Andrew Y Ng. Rectifier nonlinearities improve neural network acoustic models. In *Proceedings of the 30th International Conference on Machine Learning*, 2013.

Aravindh Mahendran and Andrea Vedaldi. Understanding deep image representations by inverting them. In *In Proceedings of IEEE Conference on Computer Vision and Pattern Recognition*, 2015.

Aravindh Mahendran and Andrea Vedaldi. Visualizing deep convolutional neural networks using natural pre-images. *International Journal of Computer Vision*, 120(3):233–255, 2016.

Stéphane Mallat. Understanding deep convolutional networks. *Philosophical Transactions of the Royal Society of London A: Mathematical, Physical and Engineering Sciences*, 374 (2065), 2016. ISSN 1364-503X. doi: 10.1098/rsta.2015.0203. URL `http://rsta.royalsocietypublishing.org/content/374/2065/20150203`.

Takeru Miyato, Toshiki Kataoka, Masanori Koyama, and Yuichi Yoshida. Spectral normalization for generative adversarial networks. In *International Conference on Learning Representations*, 2018.

Guido F Montufar, Razvan Pascanu, Kyunghyun Cho, and Yoshua Bengio. On the number of linear regions of deep neural networks. In *Advances in Neural Information Processing Systems 27*, 2014.

Maithra Raghu, Ben Poole, Jon Kleinberg, Surya Ganguli, and Jascha Sohl-Dickstein. On the expressive power of deep neural networks. In *Proceedings of the 34th International Conference on Machine Learning*, 2017.

Pau Rodríguez, Jordi Gonzàlez, Guillem Cucurull, Josep M. Gonfaus, and F. Xavier Roca. Regularizing cnns with locally constrained decorrelations. In *International Conference on Learning Representations*, 2017.

Andrew Michael Saxe, Yamini Bansal, Joel Dapello, Madhu Advani, Artemy Kolchinsky, Brendan Daniel Tracey, and David Daniel Cox. On the information bottleneck theory of deep learning. In *International Conference on Learning Representations*, 2018.

Hanie Sedghi, Vineet Gupta, and Philip M. Long. The singular values of convolutional layers. *arXiv preprint arXiv:1805.10408*, 2018.

Wenling Shang, Kihyuk Sohn, Diogo Almeida, and Honglak Lee. Understanding and improving convolutional neural networks via concatenated rectified linear units. In *Proceedings of the 33rd International Conference on Machine Learning*, 2016.

Carl-Johann Simon-Gabriel, Yann Ollivier, Bernhard Schölkopf, Léon Bottou, and David Lopez-Paz. Adversarial vulnerability of neural networks increases with input dimension. *arXiv preprint arXiv:1802.01421*, 2018.

Jure Sokolić, Raja Giryes, Guillermo Sapiro, and Miguel RD Rodrigues. Robust large margin deep neural networks. *IEEE Transactions on Signal Processing*, 65(16):4265–4280, 2017.

Christian Szegedy, Wojciech Zaremba, Ilya Sutskever, Joan Bruna, Dumitru Erhan, Ian J. Goodfellow, and Rob Fergus. Intriguing properties of neural networks. *International Conference on Learning Representations*, 2014.

Naftali Tishby and Noga Zaslavsky. Deep learning and the information bottleneck principle. In *Information Theory Workshop (ITW), 2015 IEEE*, pp. 1–5. IEEE, 2015.

Yusuke Tsuzuku, Issei Sato, and Masashi Sugiyama. Lipschitz-margin training: Scalable certification of perturbation invariance for deep neural networks. *arXiv preprint arXiv:1802.04034*, 2018.

Shengjie Wang, Abdel rahman Mohamed, Rich Caruana, Jeff Bilmes, Matthai Plilipose, Matthew Richardson, Krzysztof Geras, Gregor Urban, and Ozlem Aslan. Analysis of deep neural networks with extended data jacobian matrix. In *Proceedings of the 33rd International Conference on Machine Learning*, 2016.

A1 APPENDIX FOR SECTION 2

Proof (Corollary 2, Equivalences of omnidirectionality)
We show the equivalences by proving ***i)*** $\Rightarrow$ ***ii)*** $\Rightarrow$ ***iii)*** $\Rightarrow$ ***iv)*** $\Rightarrow$ ***i)***.
Let $A \in \mathbb{R}^{m \times n}$ be omnidirectional. Therefore, there exists a unique $x \in \mathbb{R}^n$, s.t. $Ax \leq 0$. Obviously, $x = 0$ is the solution to this inequality and we have that $\nexists x \neq 0 : Ax \leq 0$, which is identical to ***ii)***.
From ***ii)***, it follows that

$$\forall x \neq 0 \; \exists \; i \in \{1, \dots, m\} : \langle x, a_i \rangle > 0, \tag{4}$$

where a_i is the i-th row of A. Hence, for every non-zero vector x, there is a row vector a_i, that is positively correlated to x. The rows of A form the m normal vectors of the corresponding hyperplanes in $\mathbb{R}^n$. With this, equation 4 is equivalent to the fact, that every linear open halfspace in $\mathbb{R}^n$ has to contain a row of A, which is ***iii)***.
The statement in equation 4 is equivalent to

$$\begin{aligned} & \neg(\exists i \in \{i, \dots, m\} : (Ax)_i > 0) \Rightarrow \neg(x \neq 0) \\ \Leftrightarrow \; & Ax \leq 0 \Rightarrow x = 0, \end{aligned}$$

which is ***iv)***. The omnidirectionality of A is finally a simple implication of ***iv)***. Altogether, this shows the equivalence of all four points. □

Definition 10 *(Convex hull)*
For $A \in \mathbb{R}^{m \times n}$, the convex hull is defined as

$$\mathrm{Conv}(A) = \left\{ \sum_{i=1}^{m} \alpha_i a_i : \forall i \; \alpha_i \in \mathbb{R}_{\geq 0} \wedge \sum_i \alpha_i = 1 \right\},$$

where $a_i \in \mathbb{R}^n$ are the rows of A.

Theorem 11 *(Stiemke's theorem e.g. Dantzig (1963))*
Let $A \in \mathbb{R}^{m \times n}$ be a matrix, then the following two expressions are equivalent.

- $\nexists y : Ay \lneq 0$
- $\exists x > 0 : A^T x = 0$

Here $z \lneq 0$ means that $0 \neq z \leq 0$.

Theorem 12 *(Singleton solutions of inequality systems)*
Let $A \in \mathbb{R}^{m \times n}$, $b \in \mathbb{R}^m$ and $x \in \mathbb{R}^n$. Furthermore, let the inequality system

$$Ax + b \leq 0,$$

written as (A, b), have a solution x_0.
Then this solution is unique if and only if there exists an index set, I, for the rows s.t. $(A|_I, b|_I)$ is omnidirectional for x_0.

Proof (Theorem 12, Singleton solutions of inequality systems)
"$\Leftarrow$"
Let $(A|_I, b|_I)$ be omnirectional for x_0. Then it holds that $A|_I x + b|_I = A|_I (x - x_0) \leq 0$. Due to the omnidirectionality of $A|_I$, x_0 is the unique solution of the inequality system $A|_I x + b|_I \leq 0$. The existence of a solution for the whole system $Ax + b \leq 0$ is guaranteed by assumption and therefore x_0 is the unique solution of $Ax + b \leq 0$.
"$\Rightarrow$"
Here we will prove

$$\text{“}\nexists I : (A|_I, b|_I) \text{ omnidirectional for some } p \;\Rightarrow\; \text{solution non-unique”}.$$

We will start by doing the following logical transformations:

$$\begin{aligned} & \nexists I : (A|_I, b|_I) \text{ omnidirectional for some } p \\ \Leftrightarrow \; & \nexists (I, p) : (A|_I \text{ omnidirectional} \wedge b|_I = -A|_I p) \\ \Leftrightarrow \; & \forall (I, p) : \neg(A|_I \text{ omnidirectional} \wedge b|_I = -A|_I p) \\ \Leftrightarrow \; & \forall (I, p) : (A|_I \text{ not omnidirectional} \vee b|_I \neq -A|_I p). \end{aligned}$$

Now we define the vector $c_0 := Ax_0 + b \leq 0$ and the set I as the index set given via $c_0 = 0$.

This means that $A|_I$ is not omnidirectional, because otherwise $A|_I x_0 + b|_I = 0$ due to the definition of I, which would lead to the contradiction that $(A|_I, b|_I)$ is omnidirectional for x_0. But this means $\exists x' \neq 0 : A|_I x' \leq 0$ as a result of Corollary 2. Since $A|_{I^c} x_0 + b|_{I^c} < 0$, we also have $\forall x \ \exists \epsilon > 0 : A|_{I^c}(x_0 + \epsilon x) + b|_{I^c} < 0$. This holds in particular for x', so we define accordingly $x^* := \varepsilon x' \neq 0$. Therefore, we have $A|_{I^c}(x_0 + x^*) + b|_{I^c} < 0$ as well as

$$A|_I(x_0 + x^*) + b_I = \underbrace{A|_I x_0 + b_I}_{=c_0=0} + \underbrace{\varepsilon A|_I x'}_{\leq 0} \leq 0.$$

Altogether it holds that $A(x_0 + x^*) + b \leq 0$ with $x^* \neq 0$, which means that x_0 is a non-unique solution for the inequality system $Ax + b \leq 0$. □

Proof (Theorem 4, Preimages of ReLU-layers)
We consider the ReLU-layer

$$y = \mathrm{ReLU}(Ax + b),$$

given its output $y \in \mathbb{R}^m$ with $A \in \mathbb{R}^{m \times n}$, $b \in \mathbb{R}^m$ and $x \in \mathbb{R}^n$. Clearly, this equation can also be written as the mixed linear system

$$\begin{aligned} A|_{y>0} x + b|_{y>0} &= y|_{y>0}, \\ A|_{y=0} x + b|_{y=0} &\leq 0. \end{aligned}$$

This allows us to consider the two cases

$$\mathcal{N}(A|_{y>0}) = \{0\} \text{ and } \mathcal{N}(A|_{y>0}) \neq \{0\}.$$

In the first case, we have a linear system which allows us to calculate x uniquely, i.e. we can do retrieval. This leads us to the second case, the interesting one. In this case we can only recover x uniquely if and only if the system of inequalities "pins down" $P_{\mathcal{N}(A|_{y>0})} x$, where P_V is the orthogonal projection into the closed space V. Formally this requires

$$A|_{y \leq 0}(P_{\mathcal{N}(A|_{y>0})^\perp} x + P_{\mathcal{N}(A|_{y>0})} x) + b|_{y \leq 0} \leq 0$$

to have a unique solution for $x \in \mathbb{R}^n$ and $P_{\mathcal{N}(A|_{y>0})^\perp} x$ fixed (given via the equality system). By defining $\overline{b} := b|_{y \leq 0} + A|_{y \leq 0}(P_{\mathcal{N}(A|_{y>0})^\perp} x)$ we have

$$A|_{y \leq 0}(P_{\mathcal{N}(A|_{y>0})} x) + \overline{b} \leq 0.$$

If $O \in \mathbb{R}^{k \times n}$ now denotes an orthonormal basis of $\mathcal{N}(A|_{y>0})$, where $k := \dim \mathcal{N}(A|_{y>0})$, we can write

$$\overline{A}\overline{x} + \overline{b} \leq 0,$$

where $\overline{A} := AO^T$ and $\overline{x} := Ox$ is a general element in $\mathbb{R}^k$. It now follows from Theorem 12 that the inequality system $(\overline{A}, \overline{b})$ has a unique solution if and only if $(\overline{A}, \overline{b})$ has a subset of rows that are omnidirectional for some point p. □

Proof (Theorem 5, Convex hull theorem)
Since $\mathcal{N}(A) = \{0\}$ follows from both sides of the equivalence, the following sequence of equivalencies holds. $0 \in \mathrm{Conv}(A)^{\mathrm{o}} \Leftrightarrow \exists x > 0 : A^T x = 0 \xLeftrightarrow{\text{Theorem 11}} \nexists y : Ay \lneq 0$. Together with $\mathcal{N}(A) = \{0\}$, which means that $\nexists y \neq 0 : Ay = 0$, leads altogether to $\nexists y \neq 0 : Ay \leq 0$. □

A2 Proofs for section 3

Proof (Proof of Lemma 8, Global upper bound for largest/smallest singular value)
The upper bound on the largest singular value is trivial, as ReLU is contractive or in other terms $\|D_I Ax\|_2 \leq \|Ax\|_2$ for all I and $x \in \mathbb{R}^n$.
To prove the upper bound for the smallest singular value, we assume

$$\sigma_M := \min\{\sigma_l : \sigma_l > 0\} > \tilde{\sigma}_k \tag{5}$$

and aim to produce a contradiction. Consider all singular vectors $\tilde{v}_{k^*}$ with $k^* \geq k$ from matrix A. It holds for all $\tilde{v}_{k^*}$

$$\tilde{\sigma}_k \geq \tilde{\sigma}_{k^*} = \|A\tilde{v}_{k^*}\|_2 \geq \|D_I A\tilde{v}_{k^*}\|_2, \tag{6}$$

as D_I is a projection matrix and thus only contracting. As

$$\sigma_M = \min_{\substack{\|x\|_2=1 \\ x \in \mathcal{N}(D_I A)^\perp}} \|D_I A x\|_2,$$

all $\tilde{v}_{k^*} \notin \mathcal{N}(D_I A)^\perp$. Otherwise, a $\tilde{v}_{k^*}$ would be a minimizer by estimation 6, which would violate the assumption 5.

Due to $\mathcal{N}(D_I A)^\perp \oplus \mathcal{N}(D_I A) = \mathbb{R}^n$, it holds $\tilde{v}_{k^*} \in \mathcal{N}(D_I A)$. As $\tilde{v}_{k^*}$ are orthogonal, $\dim(span(v_{k^*})) = |I| + 1$ (note: $k^* = k, ..., N$ and $k = N - |I|$, thus there are $|I| + 1$ singular vectors v_{k^*} in total). Furthermore, $\tilde{v}_{k^*}$ were not in $\mathcal{N}(A)$ by definition (corresponding singular values were strictly positive).
Hence, the nullspace of D_I must have $\dim(\mathcal{N}(D_I)) \geq |I| + 1$. But D_I is the identity matrix except $|I|$ zeros on the diagonal, thus $\dim(\mathcal{N}(D_I)) = |I|$, which yields a contradiction. □

Proof (Proof of Lemma 9, Weakly correlated rows)
Consider $v = \frac{a_k}{\|a_k\|_2}$. Then,

$$(D_I A v)_k = 0,$$

since $k \in I$ (k-th row of D_I is zero). Furthermore, for all $j \neq k$ it holds by condition 3

$$(D_I A v)_j = \frac{\langle a_k, a_j \rangle}{\|a_k\|_2} \leq \frac{|\langle a_k, a_j \rangle|}{\|a_k\|_2} \leq \frac{c}{\sqrt{M}}.$$

Hence,

$$\|D_I A v\|_2 = \sqrt{\sum_{j \notin I} \left(\frac{\langle a_k, a_j \rangle}{\|a_k\|_2} \right)^2} \leq \sqrt{M \left(\frac{c}{\sqrt{M}} \right)^2} = c.$$

As $a_k \in \mathcal{N}(D_I A)^\perp$, $v \in \mathcal{N}(D_I A)^\perp$ as well. Thus,

$$\sigma_K = \min_{\substack{\|x\|_2 \\ x \in \mathcal{N}(D_I A)^\perp}} \|D_I A\|_2 \leq \|D_I A v\|_2 \leq c.$$

□

A3 APPENDIX FOR SECTION 2.2

In this section, we formulate the algorithm to determine whether the preimage of y given by

$$y = \mathrm{ReLU}(Ax + b)$$

is finite.
This requires to check whether $\overline{A}$ (see Theorem 4) is omnidirectional, which is equivalent to

$$0 \in \mathrm{Conv}(\overline{A})^{\mathrm{o}},$$

see Theorem 5. Since it is reasonable to assume that 0 will not lie on the boundary of the convex hull, we can formulate this as a *linear programming* problem. The side-conditions incorporate the definition of convex hulls (Definition 10, Appendix A1). The objective function is chosen arbitrary, as we are only interested in a solution.

Algorithm 1 Finite preimage

Input: $A \in \mathbb{R}^{m \times n}$, $b \in \mathbb{R}^m$, $y \in \mathbb{R}^m$
if $\mathrm{rank}(A|_{y>0}) = n$ **then**
  return True {Preimage is a singleton}
end if
$O \leftarrow$ orthonormal basis of $\mathcal{N}(A|_{y>0})$, $(\in \mathbb{R}^{k \times n})$
$\overline{A} \leftarrow A|_{y=0} O^T$, $(\in \mathbb{R}^{\tilde{k} \times k})$
if $\tilde{k} \leq k$ **then**
  return False {see Corollary 6}
end if
$c \leftarrow (1; \ldots; 1)$ {arbitrary objective}
return Does a solution for the linear program $\begin{cases} \max c^T x \\ \text{subject to} \\ \qquad \overline{A}^T x = 0 \\ \qquad (1; \ldots; 1)^T x = 1 \\ \qquad x \in [0,1]^{\tilde{k}} \end{cases}$ exists?

A4 ARCHITECTURES FOR NUMERICAL STUDIES

Training details for MLP on MNIST:

- Training using Adam optimizer Kingma & Ba (2015)
- Epochs: 25
- Batch size: 1000

Training details for WideCIFAR and ThinCIFAR:

- Training setup from Keras (Chollet et al., 2015) examples: `cifar10_cnn`
- No data augmentation
- RMSprop optimizer
- Epochs: 100
- Batch size: 32

Table 1: Architecture of MLP trained on MNIST

Index	Type	kernel size	stride	# feature maps	# output units
0	Input layer	-	-	3	
1	Dense layer	-	-	-	100
2	Dense layer	-	-	-	100
3	Dense layer	-	-	-	100
4	Dense layer	-	-	-	100
5	Dense layer	-	-	-	100
6	Dense layer	-	-	-	100
7	Dense layer	-	-	-	100
8	Dense layer	-	-	-	100
9	Dense layer	-	-	-	100
10	Dense layer	-	-	-	100
11	Dense layer (softmax)	-	-	-	10

Table 2: Architecture of MLP trained on MNIST

Index	Type	kernel size	stride	# feature maps	# output units
0	Input layer	-	-	3	
1	Dense layer	-	-	-	3500
2	Dense layer	-	-	-	784
3	Dense layer (softmax)	-	-	-	10

Table 3: Architecture of WideCIFAR

Index	Type	kernel size	stride	# feature maps	# output units
0	Input layer	-	-	3	
1	Convolutional layer	(3,3)	(1,1)	32	-
2	Convolutional layer	(3,3)	(2,2)	64	-
3	Convolutional layer	(3,3)	(1,1)	64	-
4	Convolutional layer	(3,3)	(1,1)	32	-
5	Convolutional layer	(3,3)	(1,1)	32	-
6	Convolutional layer	(3,3)	(2,2)	64	-
7	Dense layer	-	-	-	512
8	Dense layer (softmax)	-	-	-	10

Table 4: Architecture of ThinCIFAR

Index	Type	kernel size	stride	# feature maps	# output units
0	Input layer	-	-	3	
1	Convolutional layer	(3,3)	(1,1)	32	-
2	Convolutional layer	(3,3)	(2,2)	32	-
3	Convolutional layer	(3,3)	(1,1)	16	-
4	Convolutional layer	(3,3)	(1,1)	16	-
5	Convolutional layer	(3,3)	(1,1)	16	-
6	Convolutional layer	(3,3)	(2,2)	32	-
7	Dense layer	-	-	-	512
8	Dense layer (softmax)	-	-	-	10

A5 EFFECT OF RELU NUMERICAL ANALYSIS OF LEMMA 9

In order to better understand the bound on the smallest singular value after ReLU, given by Lemma 9, we numerically proceed as follows:

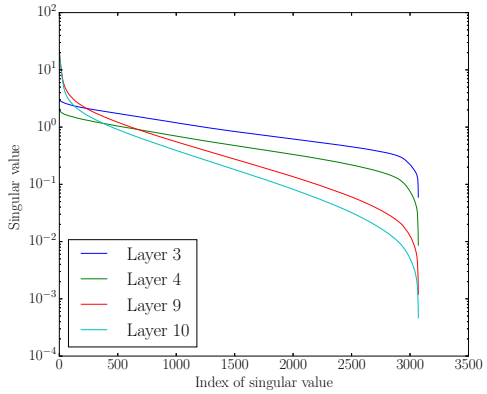

Figure 7: Effect of ReLU on the singular values for WideCifar. The curves show the effect in layer 2 (layer 3 and 4 in the legend, because ReLU is counted as an extra activation layer) and layer 5 (layer 9 and 10), where each curve is the median over 50 samples.

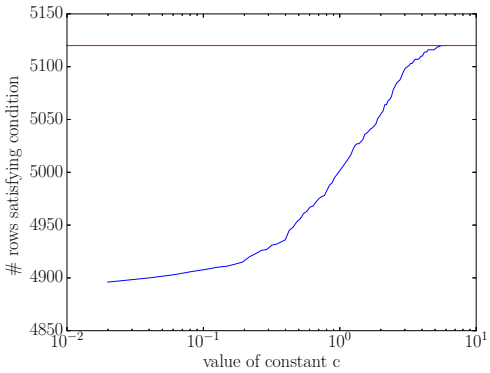

Figure 8: Curve showing how many rows a_i satisfy condition 3 from Lemma 9 depending on values of constant c. The red line shows the total number of remaining rows after removal by ReLU, $M = 5120$. Even for small constants c most a_i fulfill condition 3, yet not all, which is required by the lemma to give an upper bound on the smallest singular value. The example is from layer 4 of WideCIFAR, for only one sample from the test set.

1. We choose $c \in [a, b]$, where a, b are suitable interval endpoints.
2. Given c, we compute for every a_k with $k \in I$ the value of $c\frac{\|a_k\|_2}{\sqrt{M}}$ (M is the number of remaining rows, in the example $M = 5120$).
3. For every a_k we count the number of a_i satisfying
$$|\langle a_i, a_k\rangle| \leq c\frac{\|a_k\|_2}{\sqrt{M}}.$$
4. We take the a_k with the maximal number of a_i satisfying the condition. (Note, that this ignores the requirement $a_k \in \mathcal{N}(D_I A)^{\perp}$.)
5. If we have an a_k, where all a_i satisfy the condition, the corresponding constant c gives the upper bound on the smallest singular value after ReLU.

Figure 8 shows the number of a_i satisfying the correlation condition given different choices of c. The red line is reached for $c \approx 6$. However, even the largest singular value after ReLU is smaller than 2.5 (shown in Figure 7). Thus, the bound given by Lemma 9 is far off. This can be explained by the

fact, that this situation is quite redundant ($M = 5120$) and there are rows a_i still correlated to the removed rows a_k.
However, in the further Experiments on ThinCIFAR, we observe (see Figure A6) a stronger effect of ReLU in layer 2, which can be explained by having a less redundant scenario with fewer remaining rows.

A6 FURTHER EXPERIMENTS

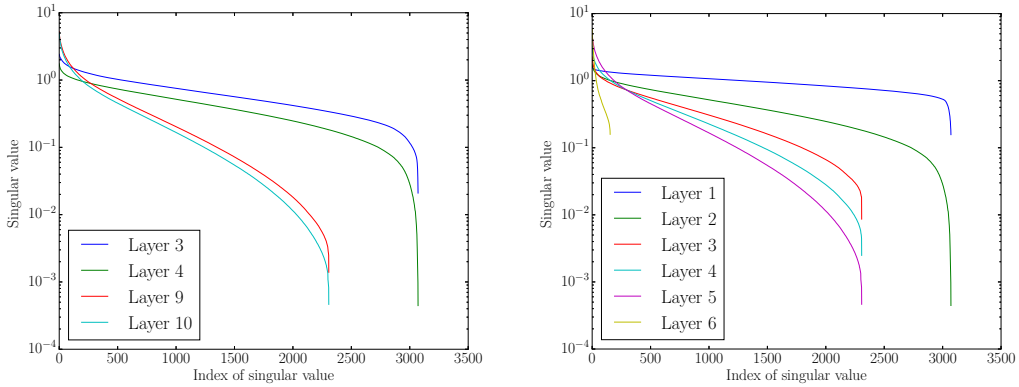

Figure 9: Left: Effect of ReLU on the singular values for ThinCifar. The curves show the effect in layer 2 (layer 3 and 4 in legend, because ReLU is counted as an extra activation layer) and layer 5 (layer 9 and 10). Right: Decay of singular values over the layers ThinCifar. Here, each layer includes the convolution and ReLU-activation. Reported number are taken from median over 50 samples. Best viewed in color.

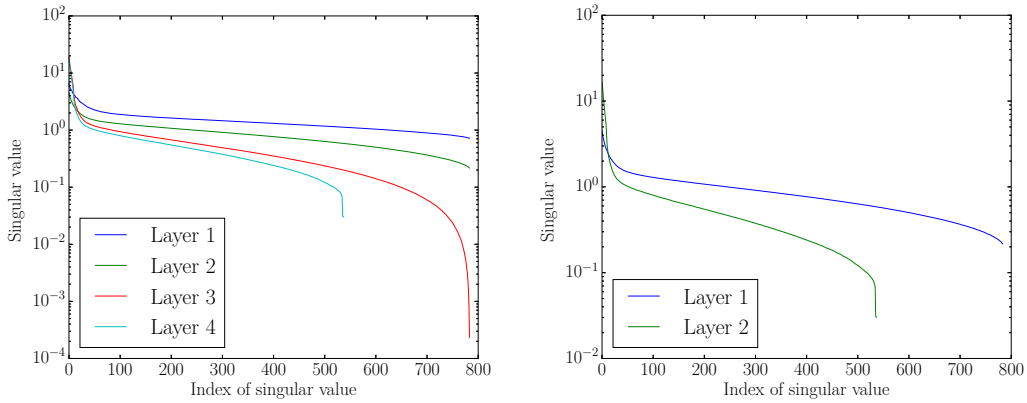

Figure 10: Left: Effect of ReLU on the singular values for the MLP on MNIST. The curves show the effect in layer 1(layer 1 and 2 in legend, because ReLU is counted as an extra activation layer) and layer 2 (layer 3 and 4). Right: Decay of singular values over the layers of MLP on MNIST. Here, each layer includes the fully-connected layer and ReLU-activation. Reported number are taken from median over 50 samples.

A7 INVARIANCE EXPERIMENT USING AN MLP ON MNIST

This section briefly describes how the results in Figure 6 from the introduction were obtained (copied in Figure 11 for readability). After training the network from 1 (in Appendix A4), we searched the MNIST test set for input images with yielded the fewest positive activations in the first layer, in the figure the digits "3" and "4". After selecting the example input x^*, we selected another input c belonging to a different class (e.g. a "6" and "4" in the first example).

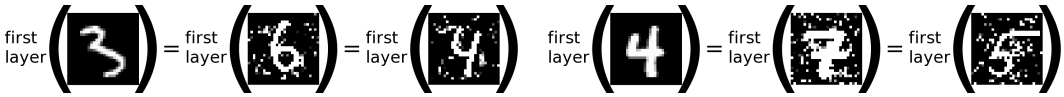

Figure 11: Invariances of the first layer (100 ReLU neurons) of a vanilla MLP. (Exact architecture in Appendix A4 Table 1.)

Afterwards, we solved following linear programming problem to find a perturbed x:

$$\begin{cases} \max \langle c, x \rangle \\ \text{subject to} \\ \qquad A|_{y^*>0} x + b|_{y^*>0} = y^*|_{y^*>0} \\ \qquad A|_{y^*<0} x + b|_{y^*<0} \leq 0 \\ \qquad x \in [0,1]^{\tilde{k}} \end{cases},$$

where the features of the first layer are computed via

$$y^* = \mathrm{ReLU}(Ax^* + b).$$

Hence, we searched within the preimage of the features y^* of the first layer for examples x which resemble images c from another class. By doing this we observe, that the preimages of the MLP may have large volume. In these cases, the network is invariant to some semantics changes which shows how the study of preimages can reveal previously unknown properties.